

UDC 669.17:539.25/27.621.374.294.18

## AN X-RAY STUDY OF THE FINE STRUCTURE AND TEXTURE OF STEEL 05G2DB AFTER CONTROLLED ROLLING

A. A. Arkhangel'skaya,<sup>1</sup> V. M. Farber,<sup>1</sup> and I. P. Konakova<sup>1</sup>

Translated from *Metallovedenie i Termicheskaya Obrabotka Metallov*, No. 9, pp. 48 – 54, September, 2014.

---

The nature of diffraction broadening of x-ray lines of pipe steel 05G2DB in various states is investigated. The pole density is computed and the most vividly manifested texture components of the sheet material of the pipe are determined.

---

**Key words:** pole density, texture, microdistortions, structure, anisotropy.

### INTRODUCTION

Gas mains are constructed from welded large-diameter pipes from steels of type 05G2DB of strength class K65(X80) [1, 2]. The possible differences in the chemical composition of the steel and process of production of sheets by the method of controlled rolling with accelerated cooling are responsible for certain deviations of the parameters of the microstructure, morphology, and phase and chemical composition of the dispersed particles after deformation. It is known that such characteristics as the homogeneity of the structure of the matrix metal determine the level of the mechanical properties of welded pipes [3].

In the present work we studied pipe steel 05G2DB with a complex structure represented by a mixture of ferrite, bainite and martensite. Depending on the gradient of the rate of cooling over the thickness of sheet, which arises under high-temperature deformation (controlled rolling) and accelerated cooling from the temperatures close to  $A_{r3}$ , the structural components may form in different combinations. The structure of a ready sheet should have a well manifested texture of deformation and transformation.

The aim of the present work was to study the parameters of the fine structure and texture of a pipe from steel 05G2DB by the x-ray diffraction method in the initial condition and after different variants of heat treatment.

### METHOD OF STUDY

We studied steel 05G2DBT with the following chemical composition (in wt.%): 0.05 C, 1.85 Mn, 0.49 Cu, 0.025 Nb, 0.016 Ti, 0.03 Mo, 0.39 Si, 0.001 S, 0.013 P.

The sheet used to weld the pipe had been produced by controlled rolling with accelerated cooling, which resulted in formation of a bainite-martensite component in the structure in addition to excess ferrite.

Test pieces of steel 05G2DBT were cut from the middle of the pipe wall. The structure of the metal was studied in the initial condition and after heat treatment by the following regimes: (1) normalizing at 900°C, 30 min, air cooling and (2) quenching from 900 (30 min) and 1100 (30 min)°C with water cooling.

The x-ray diffraction study of the fine structure was performed with the help of a DRON-3 diffractometer in cobalt  $K_{\alpha}$  radiation. The parameters of the fine structure (the size of the coherent-scattering regions (CSR) and the level of the microstresses) were determined by the method of approximation [4 – 6]. The approximating function in the analytical method was a biquadratic function  $f = \frac{1}{(1 + kx^2)^2}$ , which

gives the best approximation in description of interference lines reflected from metallic materials.

The contribution of the microdistortions and of the sizes of the CSR into the physical broadening of an interference line was computed by the Hall method by plotting the dependence of the physical broadening on the diffraction angle. The computation of the components over the coordinate axes

---

<sup>1</sup> Ural Federal University after the First President of Russia B. N. El'tsyn, Ekaterinburg, Russia (e-mail: ikonakova@rambler.ru).

depended on the kind of the approximating function used for describing the profile of the interference lines. The approximation functions were chosen in the Cauchy and Gaussian form. For the Cauchy function describing the relation  $\beta = \beta_m + \beta_n$  the values of  $\sin \theta/\lambda$  were plotted over the axis of abscissas and the values of  $\beta \cos \theta/\lambda$  were plotted over the axis of ordinates of rectangular coordinates. For the Gaussian function  $\beta^2 = \beta_m^2 + \beta_n^2$  the values of  $\sin^2 \theta/\lambda^2$  were plotted over the axis of abscissas and the values of  $\beta^2 \cos^2 \theta/\lambda^2$  were plotted over the axis of ordinates. In these formulas  $\beta$  is the physical broadening of the interference line,  $\beta_m$  is the physical broadening due to the size of the coherent-scattering region,  $\beta_n$  is the physical broadening due to the microdistortion;  $\theta$  is the Bragg angle, and  $\lambda$  is the x-ray wavelength.

We plotted the points for all the interference maximums the location of which was determined by the true width  $\beta$  in radians, angle  $\theta$ , and radiation with wavelength  $\lambda$ . Through these points we draw a straight line until intersection with the axis of ordinates. The values corresponding to the point of the intersection gave us  $1/D$  (the Cauchy function) or  $1/D^2$  (the Gaussian function); the slope ratio of the straight line to the axis of abscissas with allowance for the scale of the coordinates gives is the value of  $\Delta a/a$  (the Cauchy function) or  $\Delta a^2/a^2$  (the Gaussian function).

The size of the CSR ( $D_{HKL}$ ) and the level of the microdistortions ( $\Delta a/a$ ) were computed by the equations [4]

$$D_{HKL} = \frac{0.94\lambda}{\beta_m \cos \theta_{HKL}}; \quad (1)$$

$$\frac{\Delta a}{a} = \frac{\beta_n}{4 \operatorname{tg} \theta_{HKL}}, \quad (2)$$

where  $\theta_{HKL}$  is the Wouff-Bragg angle for the chosen interference lines  $HKL$ .

The standard was an annealed piece of armco iron, in which the broadening of the interference maximums was instrumental. To determine the physical broadening of the interference maximums from the broadening of the interference maximums obtained in the diffraction patterns of the studied specimen we computed the instrumental broadening using approximating functions.

To determine the texture components we computed the pole density, which described the fraction of the crystalline grains with the  $\{hkl\}$  planes arranged in parallel to the rolling plane. The pole density (or the density of the normal to planes  $\{hkl\}$  in a textured specimen) was determined by the formula [4]

$$P_{hkl} = \frac{J_{HKL}^t \sum J_{HKL}^{nt}}{J_{HKL}^{nt} \sum J_{HKL}^t}, \quad (3)$$

where  $J_{HKL}^t$  is the integral intensity of the  $HKL$  maximum of the textured specimen,  $\sum J_{HKL}^t$  and  $\sum J_{HKL}^{nt}$  are the sums of the

integral intensities of the  $HKL$  maximums of one order of reflection in the diffraction pattern of the textured and non-textured specimens, respectively, and  $J_{HKL}^{nt}$  is the integral intensity of the  $HKL$  maximum in the diffraction pattern of the non-textured specimen.

The integral intensity of the interference maximums (lines) in the diffraction pattern of a non-textured (random-orientation) specimen was computed from the diffraction pattern of the standard (annealed armco iron).

In addition to the specimens in the initial condition cut from the middle of the pipe wall we also studied specimens after normalizing, where the dominant structural component was polygonal ferrite, and after quenching from 900 and 1100°C, where the dominant component was bainite/martensite.

## RESULTS AND DISCUSSION

In the studied super-low-carbon steel 05G2DBT the bainite and the martensite have a bcc lattice, just like the ferrite, and the lattice constants of the former two are close to those of the latter. The tests performed have shown that reflection from the planes of these phases produces an integral diffraction pattern with symmetric interference maximums from similar planes, the reflection (Wouff-Bragg) angles of which have the same values (Table 1).

We computed the broadening of all the interference maximums due to reflection from the standard specimen and from all the planes of the experimental specimens. This was necessary because the effects of the broadening of the x-ray lines were analyzed analytically in terms of the lines of two orders of reflection and graphically by the Hall method, which requires data on the physical broadening of all the interference maximums in the diffraction pattern for the plot.

The results of the computation of the physical broadening of the interference maximums in the diffraction patterns are presented in Table 1. The analytical method was used to compare the physical broadening of the interference maximums  $\beta_{220}/\beta_{110}$ . In this case the sizes of the CSR and of the microdistortions were computed from lines of two orders. It turned out that the ratio of the physical broadening of the diffraction lines ( $\beta_{220}/\beta_{110} \geq 3.8$ ) was critical for the steel in the initial, normalized, and quenched (from 1110°C) conditions. It is commonly assumed that at this ratio the size of the CSR is about 0.15  $\mu\text{m}$  and larger [4]. The computed sizes of the CSR exceed the values permissible for the chosen model and reflected the values averaged for the ferrite grains, where the flaw density was not high, and for the regions with bainitic and martensitic structure with a high flaw density.

This allowed us to infer that the physical broadening of the interference lines for steel 05G2DBT is chiefly caused by microdistortions. In only one case a specimen quenched from 900°C had a ratio  $\cos \theta_{110}/\cos \theta_{220} < \beta_{220}/\beta_{110} < \tan \theta_{220}/\operatorname{tg} \theta_{110}$ , which was equal to  $1.90 < 3.44 < 3.81$ . In this case we computed the contributions introduced by the

**TABLE 1.** Physical Broadening of Interference Lines ( $\beta$ ) of Steel 05F2MB after Different Variants of Heat Treatment

Heat treatment	{ <i>HKL</i> }	$\theta$ , deg	$\beta \times 10^{-3}$ , rad	$\beta_{220}/\beta_{110}$	$\cos \theta_{110}/\cos \theta_{220}$	$\tan \theta_{220}/\tan \theta_{110}$
Initial condition	110	26.15	1.33	6.05	2.00	3.89
	200	38.50	6.04			
	211	49.87	10.71			
	220	61.82	8.02			
Normalizing at 900°C	110	26.12	1.21	4.68	1.90	3.81
	200	38.51	4.35			
	211	49.76	4.15			
	220	61.83	5.67			
Quenching from 900°C	110	26.12	5.54	3.44	1.90	3.81
	211	49.75	12.88			
	220	61.87	19.06			
Quenching from 1100°C	110	26.14	4.65	3.80	1.90	3.81
	211	49.79	14.09			
	220	61.87	17.71			

microstresses and by the sizes of the CSR into the physical broadening of the x-ray lines using a nomogram. The elastic stresses were evaluated in terms of the mean value of the modulus of elasticity for a polycrystalline condition of  $\alpha$ -iron, i.e.,  $E_m = 210,000$  MPa [6].

The results of the analysis of the fine structure showed that the CSR of the steel in all the conditions studied were large ( $> 150$  nm), and the main contribution into the physical broadening of the interference maximums (Table 2) was introduced by microstresses that caused microdistortions.

Figure 1 presents the dependences of  $\beta \cos \theta / \lambda$  on  $\sin \theta / \lambda$  for steel 05G2DBT after different variants of treatment. It can be seen that these functions are not suitable for determining the value of  $1/D$  due to the large sizes of the CSR. This agrees with the results of the analytical computation and proves that the main contribution into the physical broadening of the interference lines is made by microstresses.

The physical broadening of the diffraction lines of the specimens studied was determined with the help of a bi-quadratic function used as an approximating one. This characteristic has close but intermediate values as compared to

the physical broadening computed with the use of the Cauchy and Gaussian equations as the approximating functions. This makes it possible to compare the results of the computation of the microdistortions and of the CSR sizes performed analytically from diffraction lines of two orders of reflection and graphically by the Hall method.

The curves plotted with the use of the Cauchy and Gaussian functions for the specimens after normalizing and quenching are similar and differ little from each other by the slope to the axis of abscissas. For this reason we will present and analyze the plots obtained for the Cauchy approximation function

$$\beta = \frac{\lambda}{D \cos \theta} + 4 \frac{\Delta a}{a} \operatorname{tg} \theta \quad \text{or} \quad \frac{\beta \cos \theta}{\lambda} = \frac{1}{D} + 4 \frac{\Delta a}{a} \frac{\sin \theta}{\lambda} \quad (4)$$

The linear relations for all the analyzed kinds of heat treatment pass through the points corresponding to each interference maximum in the diffraction pattern, the position of

**TABLE 2.** Values of CSR and Relative Microdeformation Computed from Interference Lines of Two Orders of Reflection for Steel 05G2MB after Different Variants of Heat Treatment

Heat treatment	{ <i>HKL</i> }	$\beta_m^{110} \cdot 10^{-3}$ , rad	$D$ , nm	$\beta_n^{220} \times 10^{-3}$ , rad	$\Delta a/a \times 10^{-3}$	$\sigma$ , MPa
Initial condition	110		$\gg 150$		1.05	221
	220	–		8.03		
Normalizing at 900°C	110	–	$\gg 150$		0.76	160
	220	–		5.67		
Quenching from 900°C	110	1.27	157.8		2.27	476
	220	–		16.96		
Quenching from 1100°C	110	–	$\gg 150$		1.58	498
	220	–		17.71		

**TABLE 3.** Level of Microdistortions ( $\Delta a/a$ ) in Steel 05G2MB after Different Variants of Heat Treatment

Heat treatment	$\Delta a/a \times 10^{-3}$	
	Analytical method	Hall method
Initial condition	1.05	4.66
Normalizing at 900°C	0.76	1.01
Quenching from 900°C	2.27	2.99
Quenching from 1100°C	1.58	2.98

which on the plot is determined by the diffraction angle and by the physical broadening of the given maximum.

Table 3 presents the results of the computation of microdistortions in the steel. The values of the microdistortions obtained analytically and by the graphic method exhibit a common tendency of changes depending on the heat treatment variant of steel 05G2DBT but differ in the absolute values. The microdistortions computed by the Hall method are higher than those determined by the analytical method. For example, the microdistortions computed by the Hall method for the steel normalized and quenched from 900°C are about 1.3 times higher and those computed for the steel quenched from 1100°C are about twice higher than the analytically obtained values.

The only exception is the specimen cut from the pipe in the initial condition. The points of the Hall plot corresponding to the interference maximums obtained due to reflection from the planes of this specimen are too scattered for drawing a straight line (see Fig. 1).

It should be noted that the points obtained deviate from a rectilinear dependence to this or that degree both for normalized and for quenched steel 05G2DBT depending on the heat treatment conditions. However, for all the heat treated specimens the location of the points in the Hall diagram, which is determined by the physical broadening of the interference maximums, is well describable by a linear characteristic in contrast to the specimen in the initial condition. Straight line 2 plotted for steel 05G2DBT after normalizing passes through the points matching the  $\{110\}$ ,  $\{211\}$  and  $\{220\}$  maximums with an inconsiderable deviation.

For the steel quenched from 900°C all the points corresponding to the  $\{110\}$ ,  $\{211\}$  and  $\{220\}$  maximums match one straight line 3 without deviation. For the steel quenched from 1100°C the points are scattered considerably with respect to straight line 4 drawn between them (see Fig. 1).

The Hall plots reflect the structural state formed in the sheet as a result of the production and after different variants of heat treatment [7–10]. In a sheet with a ferrite-bainite/martensite structure obtained by controlled rolling with accelerated cooling texture arises as a result of several processes, namely, (1) hot deformation of austenite under intense plane-parallel rolling of the sheet in several passes at a temperature above  $A_{r1}$  and in the intercritical temperature range (ITR), (2) recrystallization of the austenite (dynamic

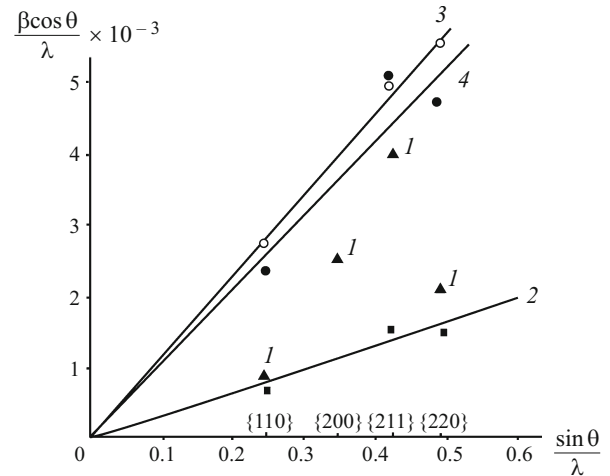


**Fig. 1.** Hall functions for steel 05G2MB plotted with the use of the Cauchy function for determining the size of the CSR and the values of the microdistortions: 1 ( $\blacktriangle$ ) – initial state; 2 ( $\blacksquare$ ) – normalizing; 3 ( $\circ$ ) – quenching from 900°C; 4 ( $\bullet$ ) – quenching from 1100°C.

in the rolls and static in the pauses between the passes) during the rough and finish rolling, (3) deformation of the ferrite, when it ends in the ITR, and (4) formation of products of decomposition of hot-rolled or recrystallized austenite in cooling of the sheet.

We may infer that the dominant orientation of crystals in sheets produced by controlled rolling with accelerated cooling is a combination of the texture of hot-deformed austenite inherited by the polygonal ferrite, bainite and/or martensite and the texture of ferrite, when the plastic deformation is finished at a temperature below  $A_{r3}$ .

In addition the formation of a structure characterized by dominant orientation of crystallites (grains) in steel 05G2DBT should lead to considerable anisotropy of the properties of the polycrystalline material, which exerts a directed action on its microstress state and the related microstrain.

In this connection, we computed the pole density for planes  $\{hkl\}$  of steel 05G2DBT in different conditions and estimated the texture formed. We also analyzed the microdistortions and microdeformations for every interference maximum in the diffraction patterns of specimens treated by different regimes.

The values of the microdistortions obtained by the method of approximation (Table 3) in the heat treated specimens were average ones for the irradiated microvolumes and were determined for a quasi-isotropic condition of the crystalline material. To evaluate the elastic stresses we used the mean value of the modulus of elasticity for polycrystalline  $\alpha$ -iron, i.e.,  $E_m = 210,000$  MPa [6].

A deformed polycrystalline material such as steel 05G2DBT with a structure formed during rolling of a sheet has a well manifested orientation of the crystals and is not an elastically isotropic one. It is necessary to take into account the anisotropy over different crystallographic directions with

**TABLE 4.** Physical Broadening ( $\beta$ ), Microdistortions  $\Delta a/a$ , Microstresses ( $\sigma$ ) Computed from Different Interference Maximums  $\{HKL\}$  for Steel 05G2MB after Different Variants of Heat Treatment

Heat treatment	$\theta$ , deg	$\beta$	$\tan \theta$	$\Delta a/a \times 10^{-3}$	$\dot{A}_{HKL} \times 10^4$ MPa	$\sigma$ , MPa
Initial condition	110	26.15	1.33	0.4910	0.68	22.50
	200	38.50	6.04	0.7954	1.90	13.43
	211	49.87	10.71	1.1854	2.26	22.50
	220	61.82	8.02	1.8660	1.07	22.50
Normalizing at 900°C	110	26.12	1.21	0.4903	0.62	22.50
	200	38.51	4.35	0.7954	1.37	13.43
	211	49.79	4.15	1.1812	0.88	22.50
	220	61.83	5.67	1.8680	0.76	22.50
Quenching from 900°C	110	26.12	5.54	0.4903	2.82	22.50
	211	49.75	12.88	1.1830	2.72	22.50
	220	61.87	19.06	1.8700	2.55	22.50
Quenching from 1100°C	110	26.14	4.65	0.4906	2.37	22.50
	211	49.49	14.09	1.1833	2.98	22.50
	220	61.87	17.71	1.8700	2.37	22.50

an obligatory correction for the modulus of elasticity  $E_{hkl}$  for different reflecting planes ( $hkl$ ).

For the crystals with a cubic lattice [5]

$$\frac{1}{E_{hkl}} = S_{11} - 2 \left[ (S_{11} - S_{12}) - \frac{1}{2} S_{44} \right] \times \frac{h^2 k^2 + k^2 l^2 + l^2 h^2}{(h^2 + k^2 + l^2)^2}, \quad (5)$$

where  $h$   $k$   $l$  are the indexes (directions) of the reflecting plane;  $S_{11}$ ,  $S_{12}$ ,  $S_{44}$  are the coefficients of elasticity entering the matrix relating the stresses and the strains characterizing the resistance of the lattice to the active stresses.

We used the experimental values of the elastic constants for  $\alpha$ -Fe presented in [5] to compute  $hkl$  over different directions in the bcc lattice, i.e.,  $E_{100} = 13.43 \times 10^4$  MPa,  $E_{110} = 22.50 \times 10^4$  MPa, and  $E_{211} = 22.50 \times 10^4$  MPa.

With allowance for the anisotropy of the lattice of the studied steel in the initially deformed condition we determined the physical broadening  $\beta_{HKL}$  for all the interference maximums  $\{hkl\}$  in the diffraction patterns of the specimens after the chosen heat treatment variants. Using the earlier made conclusion that the main contribution into the physical broadening of the maximums is introduced by the microdistortions of the lattice we computed the microstrains and microstresses by the formulas

$$\left( \frac{\Delta a}{a} \right)_{HKL} = \frac{\beta_{HKL}}{4 \operatorname{tg} \theta_{HKL}}; \quad \sigma_{HKL} = E_{HKL} \left( \frac{\Delta a}{a} \right)_{HKL}. \quad (6)$$

It can be seen from Table 4 that the physical broadening of the interference maximums in the diffraction patterns of the studied steel in the initial condition and after the heat treatment and the corresponding microstrains differ for dif-

ferent crystallographic directions  $\langle HKL \rangle$ . This is especially vivid when we compare the microdistortions ( $\Delta a/a$ ) over directions  $\langle 110 \rangle$  and  $\langle 211 \rangle$  of the  $\alpha$ -phase taking into account that the moduli of elasticity  $E_{110}$  and  $E_{211}$  have the same value.

In the initial condition (in the pipe) the highest elastic distortions are observed only over directions  $\langle 211 \rangle$  of the  $\alpha$ -phase; they are three times higher than the microdistortions over directions  $\langle 110 \rangle_{\alpha}$ .

Normalizing of steel 05G2DBT reduces markedly the anisotropy in the lattice and produces a virtually quasi-isotropic stress state.

It should be noted that the microdistortions in directions  $\langle 100 \rangle$  of the  $\alpha$ -phase are quite high both in the initial condition of the steel and after normalizing. However, the modulus of elasticity  $E_{100}$  is almost twice lower than  $E_{110}$ , which causes commensurable microstresses in planes  $\{100\}_{\alpha}$  and  $\{110\}_{\alpha}$ .

Quenching of the steel from 900°C as well as normalizing at 900°C also reduces markedly the anisotropy in the lattice of the initial polycrystal with directed orientation of crystallites (grains) and creates an almost quasi-isotropic state in the latter.

Increase of the temperature of heating for quenching to 1100°C again enhances noticeably the anisotropy in the lattice of the polycrystal with directed orientation of grains in the structure and causes growth of the microdistortions in directions  $\langle 211 \rangle$  of the  $\alpha$ -phase as compared to the microdistortions over direction  $\langle 110 \rangle_{\alpha}$ .

The conclusions following from the analysis of microstrains and microstresses performed with allowance for the anisotropy in the lattice of the polycrystalline material with an oriented form of grains in the structure coincide completely with the conclusions drawn from the analysis of the

**TABLE 5.** Pole Density of Planes  $\{hkl\}$  in Steel 05G2MB after Different Variants of Heat Treatment

Heat treatment	Pole density		
	$P_{\{110\}}$	$P_{\{100\}}$	$P_{\{211\}}$
Initial condition	0.43	1.44	2.44
Normalizing at 900°C	0.35	1.09	1.59
Quenching from 900°C	0.79	–	1.67
Quenching from 1100°C	0.47	–	2.70

plot constructed by the Hall method and reflecting the state of the metal in the specimens of the pipe with the initial structure and after different variants of heat treatment.

In the present work we have dealt primarily with the texture formed in the steel as a result of metallurgical production and after heat treatment.

Table 5 presents the pole density for planes  $\{hkl\}$  after different treatment variants. It can be seen that in the initial specimen the pole density of planes  $\{100\}$  and  $\{211\}$  is much higher than that of plane  $\{110\}$  as compared to the normalized condition. The pole density for planes  $\{211\}$  exceeds that for planes  $\{100\}$  noticeably.

Judging by the results obtained, the hot-deformed austenite of the studied steel possesses at least two components  $\{110\}_\gamma$ ,  $\{112\}_\gamma$  and  $\{112\}_\gamma$ ,  $\{111\}_\gamma$  of deformation texture, which transform into texture components  $\{001\}_\alpha$ ,  $\langle 110 \rangle_\alpha$  and  $\{112\}_\alpha$ ,  $\langle 110 \rangle_\alpha$ , respectively, under the shear transformation of the austenite into an  $\alpha$ -phase (martensite or bainite).

The structure of the steel in the initial state is represented by a mixture of ferrite, martensite and bainite and has a well manifested deformation texture. As we have shown above, this affects differently the broadening of the interference lines with different  $\{hkl\}$  indexes and the values of the microstrains and microstresses (Table 4). Both the pole density  $P_{\{211\}}$  and the microdistortions in directions  $\langle 211 \rangle$  are several times higher than the respective values for directions  $\langle 110 \rangle$  and  $\langle 100 \rangle$  in the initial specimens. The presence of a strong texture also explains the scattering of points in the Hall plot for these specimens, which excludes drawing of a straight line through them (see Fig. 1).

Normalizing at 900°C partially breaks the deformation texture, reduces the fraction of oriented crystals in the structure of the steel, and thus lowers considerably the pole density for planes  $\{100\}$  and  $\{211\}$ . The points computed for plotting the Hall diagram for the normalized steel, which correspond to interference maximums  $\{110\}$ ,  $\{211\}$  and  $\{220\}$ , match a straight line with inconsiderable deviations. The small slope of this line to the axis of abscissas indicates a low level of microstresses in the steel. This is also connected with the decrease in the anisotropy of microstrain in different planes to an almost quasi-isotropic condition of the specimen (Table 4).

It should be noted that we have observed quite high microdistortions in directions  $\langle 100 \rangle$  of the  $\alpha$ -phase in steel 05G2DBT both in the initial condition and after normalizing. However, the modulus of elasticity  $E_{100}$  is almost twice lower than  $E_{110}$ , which makes the values of the microstresses in different directions of the crystallographic lattice ( $\langle 100 \rangle_\alpha$ ,  $\langle 110 \rangle_\alpha$ ,  $\langle 211 \rangle_\alpha$ ) of the textured polycrystal commensurable.

The pole densities  $P_{\{211\}}$  of the steel after normalizing and after quenching from 900°C are close, while the pole density  $P_{\{110\}}$  in the quenched steel is twice higher than that of the normalized one. The level of the microdistortions in the steel quenched from 900°C is about 3 times higher than in the normalized one, though its deformed condition after such a treatment may be described as a virtually pseudo-isotropic one (Table 4). For this reason, straight line 3 in the Hall diagram (see Fig. 1) passes through all the points matching the  $\{110\}$ ,  $\{211\}$  and  $\{220\}$  maximums. The high level of microdistortions in the structure of the steel quenched from 900°C is caused by the high density of the lattice flaws of the products of the shear transformation of the austenite (bainite and martensite).

After quenching from 1100°C the pole density for planes  $\{211\}$  increases again, and its values are higher than for planes  $\{211\}$  of the steel in the initial condition. In addition, steel 05G2DBT both in the initial condition and after quenching from 1100°C is characterized by a high level of microdistortions and enhanced anisotropy in the lattice at the highest microdistortions in directions  $\langle 211 \rangle$  (Table 4). The Hall diagram exhibits great deviations of the points corresponding to the  $\{110\}$ ,  $\{211\}$  and  $\{220\}$  maximums from straight line 4 (see Fig. 1). This means that the processes of texture formation caused by the shear orientation rearrangement of the austenite into martensite and/or bainite, which occurs in cooling from a much higher temperature (as compared to quenching from 900°C) and gives rise to a more developed transformation texture, have intensified.

Thus, we have detected well manifested influence of the deformation and transformation texture on the diffraction pattern in a polycrystalline material with directed oriented crystallites. The structure of such a polycrystalline material with directed oriented phase components (in contrast to their equiaxed precipitation) not only changes the integral intensity of maximums in the respective diffraction patterns and the pole density, but also affects to this or that degree their physical broadening. This causes changes in the values of microdistortions in different crystallographic directions of the lattice, which makes it possible to determine and estimate the anisotropy of the properties of the polycrystalline material.

## CONCLUSIONS

1. Broadening of the interference lines of the  $\alpha$ -phase (bainite, martensite and ferrite) in the diffraction patterns of specimens of steel 05G2MB cut from a welded pipe in the

initial condition and after normalizing and quenching from different temperatures is chiefly a result of microdistortions.

2. The structure of steel 05G2MB with directed oriented phase components (in contrast to equiaxed phase precipitation) influences differently the physical broadening of the diffraction lines with different  $\{HKL\}$  indexes.

3. Analysis of the pole density  $P_{hkl}$  has shown that in the initial condition of the pipe from steel 05G2MB there forms a dominant orientation of planes  $\{100\}$  and  $\{211\}$  of the  $\alpha$ -phase, which is preserved after normalizing and quenching.

4. The texture component characterized by pole density  $P_{100}$  is inherited by the  $\alpha$ -ferrite from the hot-deformed austenite; the high values of pole density  $P_{211}$  are a result of the contribution of the deformation texture of the ferrite and of the texture due to the shear transformation developed during the formation of bainite and martensite.

*The authors are grateful to L. D. Chumakova for the useful advices and help with the work presented.*

## REFERENCES

1. A. B. Arabey, "Development of specifications for the metal of pipes for cross-country pipelines," *Izv. Vysh. Uchebn. Zaved., Chern. Metall.*, No. 7, 3 – 10 (2010).
2. I. Yu. Stolyarov, A. M. Gervas'ev, et al., "Special features of structure and properties of experimental batches of pipes of strength category K65 (X80) prepared for complex tests," *Nauka Tekh. Gaz. Prom-sti*, No. 1, 56 – 61 (2009).
3. I. N. Ashikhmina, S. V. Belikov, A. I. Stepanov, and K. I. Sergeeva, "Laws of structure formation in heat treatment of oil pipes with enhanced operating reliability fabricated from steel 13KhFA," *Stal'*, No. 3, 62 – 65 (2013)
4. Ya. S. Umanskii, Yu. A. Skakov, A. N. Ivanov, and L. N. Rastorguev, *X-ray and Electron-Optical Analysis (A Tutorial)* [in Russian], MISiS, Moscow (2002), 360 p.
5. Yu. A. Bogoryadskii (ed.), *Radiography in Physical Metallurgy* [in Russian], Gos. Nauch. Izd. Liter. Chern. Tsvetn. Metall., Moscow (1961).
6. A. Taylor, *X-ray Metallography* [Russian translation], Metallurgiya, Moscow (1965), 377 p.
7. Ogawa R. Jutori, "Texture and toughness of steel pipes designed by controlled rolling," *Kobe Steel Eng. Rep.*, **31**(1), 57 – 61 (1981).
8. S. S. Gorelik, S. V. Dobatkin, and L. M. Kaputkina, *Recrystallization of Metals and Alloys* [in Russian], MISiS, Moscow (2005), 432 p.
9. I. Yu. Pyshmintsev, M. A. Smirnov, A. N. Mal'tseva, et al., "Structure and properties of low-carbon pipe steels subjected to pneumatic tests," *Stal'*, No. 2, 75 – 81 (2011).
10. V. M. Schastlivtsev, T. I. Tabatchikova, I. D. Yakovleva, et al., "Effect of texture on the cold resistance of a weldable steel subjected to thermomechanical treatment," in: *Deformation and Fracture of Metals* [in Russian], URO RAN, Ekaterinburg (2010), pp. 34 – 40.